J. Fluid Mech. (2013), *vol.* 727, *pp.* 161–190.
doi:10.1017/jfm.2013.233

Spatial variations of magnetic permeability as a source of dynamo action

B. Gallet†, F. Pétrélis and S. Fauve

Laboratoire de Physique Statistique, École Normale Supérieure CNRS UMR8550, 24 rue Lhomond, F-75005 Paris, France

(Received 21 June 2012; revised 28 February 2013; accepted 6 May 2013; first published online 19 June 2013)

We investigate dynamo action for a parallel flow of an electrically conducting fluid located over a boundary with spatially varying magnetic permeability. We first compute the dynamo threshold numerically. Then we perform an asymptotic expansion in the limit of small permeability modulation, which gives accurate results even for moderate modulation. We present in detail the mechanism at work for this dynamo. It is an interplay between shear (an ω-effect) and a new conversion mechanism that originates from the non-uniform magnetic boundary. We illustrate how a similar mechanism leads to dynamo action in the case of spatially modulated electrical conductivity, a problem studied by Busse & Wicht (*Geophys. Astrophys. Fluid Dyn.*, vol. 64, 1992, pp. 135–144). Finally, we discuss the relevance of this effect to experimental dynamos and present ways to increase the dynamo efficiency and reduce the instability threshold.

Key words: bifurcation, dynamo theory, MHD and electrohydrodynamics

1. Introduction

Dynamo action is the transformation of mechanical work into electromagnetic energy without the use of permanent magnetism or an external current source. It is an instability process that amplifies perturbations of current or magnetic field, when electromagnetic induction due to the motion of an electrically conducting medium overcomes Ohmic dissipation. This process has been used since the end of the nineteenth century to generate electricity from mechanical work (Siemens 1867). In these widely used rotor dynamos, the current lines are imposed by electric wiring and the geometry of magnetic field lines is constrained by ferromagnetic material. If high-magnetic-permeability material were not used, these rotor dynamos could in principle still operate, but for much higher rotation rates that are rather difficult to achieve in simple devices. It was first proposed by Larmor (1919) that the magnetic field of the sun is also generated through a dynamo process by the flow of an electrically conducting fluid. It is now believed that the magnetic field of most planets and stars is generated by dynamo action. In contrast to rotor dynamos, these geophysical or astrophysical ones are homogeneous dynamos, i.e. the electrical conductivity and the magnetic permeability of the fluid are assumed to be constant within the whole flow domain. This makes the dynamo mechanism much more difficult to describe.

† Email address for correspondence: basile.gallet@gmail.com

In addition, it has been found that magnetic fields with too many symmetries cannot be generated by dynamo action (Cowling 1933; Lortz 1968) and that too simple flows, for instance planar flows, cannot generate a magnetic field (Zel'dovich 1957). However, planetary and stellar interiors involve gradients of temperature, density and chemical composition, thus making homogeneous models questionable. It was proposed that a spatially dependent electrical conductivity can favour dynamo action. A model was studied by Busse & Wicht (1992), who showed that the simplest flow with a uniform velocity field along a boundary with spatially periodic variation of electrical conductivity can generate magnetic field.

Interest in this type of dynamo has been motivated again recently, following the observation of a magnetic field generated by a von Kármán swirling flow of liquid sodium (VKS experiment: Monchaux *et al.* 2009). Indeed, within the limited parameter range of the experiment, dynamo action has been observed so far only when propellers made of iron are used to drive the flow. These propellers consist of iron disks fitted with eight iron blades, thus involving a spatially periodic variation of magnetic permeability. It has been proposed by Giesecke, Stefani & Gerbeth (2010) that this could favour dynamo action in the VKS experiment. Although this is not the only possible mechanism, it is worth studying it in order to evaluate how realistic it could be. Part of the results reported in this study were announced in Gallet, Pétrélis & Fauve (2012) and are presented here in detail.

The paper is organized as follows: in § 2, we present a simple model analogous to the one of Busse & Wicht (1992): a uniform flow of an electrically conducting fluid along a boundary with a spatially periodic magnetic permeability. The kinematic dynamo problem is solved numerically in § 3. We show that a dynamo is generated in this configuration and study how its threshold depends on the width of the boundary and on the modulation of magnetic permeability. The structure of the most unstable eigenmode and the nature of the bifurcation are analysed in § 4. The problem is solved analytically in § 5 in the limit of small-amplitude modulation and the mechanism for dynamo action is explained. We show that a similar mechanism operates in the case of a spatial modulation of electrical conductivity studied by Busse & Wicht (1992). In § 6 we discuss the relevance of this mechanism for the VKS experiment. We conclude in § 7 with a discussion of our results in the framework of spatial symmetries and anti-dynamo theorems.

2. A minimal model

In figure 1 we consider a system similar to the one in Busse & Wicht (1992), but in which the magnetic permeability of the boundary is modulated in space while the electrical conductivity is constant: a fluid of electrical conductivity σ and magnetic permeability μ_0 flows uniformly with a velocity $U\boldsymbol{e_x}$ in the semi-infinite space $\tilde{z} > 0$. Under this fluid is a rigid boundary of the same electrical conductivity, and of magnetic permeability $\mu_r(\tilde{x})\mu_0$, with $\mu_r(\tilde{x}) = m_0 + m_1 \sin(\tilde{x}/L)$, where m_0 is the mean magnetic permeability, and m_1 and $2\pi L$ are the amplitude and wavelength of the permeability modulation. Denoting as D the dimensionless thickness of this modulated boundary, it extends down to $\tilde{z} = -DL$, under which is a medium of infinite magnetic permeability. The boundary being at rest, there is an infinite shear at $\tilde{z} = 0$ which converts magnetic field perpendicular to the boundary into magnetic field parallel to the flow.

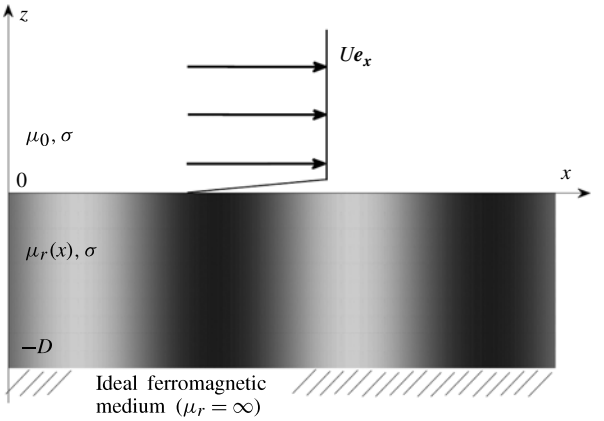

FIGURE 1. A minimal model: an infinite shear at the interface between an electrically conducting fluid and a boundary of spatially modulated magnetic permeability.

2.1. *Induction equation with space varying permeability*

We use L and $\mu_0\sigma L^2$ as length and time scales, and define the magnetic Reynolds number as $Rm = \mu_0\sigma UL$. Denoting without a tilde the dimensionless coordinates, the induction equation inside the fluid reads

$$\partial_t \boldsymbol{B} + Rm\partial_x \boldsymbol{B} = \Delta \boldsymbol{B}, \tag{2.1}$$

where Δ is the Laplacian operator. Inside the modulated boundary, the Maxwell–Faraday equation together with Ohm's law yields

$$\mu_r \partial_t \boldsymbol{H} = -\boldsymbol{\nabla} \times (\boldsymbol{\nabla} \times \boldsymbol{H}), \tag{2.2}$$

with $\boldsymbol{B} = \mu_0\mu_r\boldsymbol{H}$. This gives only two independent scalar relations, the third one coming from the zero divergence of $\boldsymbol{B}$:

$$\boldsymbol{\nabla} \cdot (\mu_r \boldsymbol{H}) = 0. \tag{2.3}$$

The problem being translation-invariant in the y-direction, the Fourier modes in this direction decouple. Let us consider an eigenmode $\boldsymbol{H}\mathrm{e}^{st}\mathrm{e}^{iky}$, where $\mathrm{Re}(s)$ is the growth rate, $\mathrm{Im}(s)$ is the angular frequency, and k is the wavenumber in the y-direction. Equation (2.3) gives H_y in terms of H_x and H_z. This expression for H_y is used in the x- and z-components of (2.2) to get the two coupled equations

$$\mu_r^3 s H_x = \mu_r^2(\partial_{xx}H_x - k^2 H_x + \partial_{zz}H_x) + (\mu_r''\mu_r - (\mu_r')^2)H_x + \mu_r\mu_r'\partial_x H_x, \tag{2.4}$$

$$\mu_r^2 s H_z = \mu_r(\partial_{xx}H_z - k^2 H_z + \partial_{zz}H_z) + \mu_r'\partial_z H_x, \tag{2.5}$$

where $\mu_r(x) = m_0 + m_1 \sin x$ and μ_r' is its x-derivative.

2.2. *Solution inside the fluid and boundary conditions*

We want to solve (2.4) and (2.5) analytically or numerically. The boundary conditions at $z = -D$ are $H_x = 0$ and $H_y = 0$, which gives $\partial_z H_z = 0$ using (2.3). The matching relations at the fluid–boundary interface $z = 0$ are:

(i) continuity of the normal component of $\boldsymbol{B}$: $B_z|_{0^+}/\mu_0 = \mu_r H_z|_{0^-}$;

(ii) continuity of H_x: $B_x|_{0^+}/\mu_0 = H_x|_{0^-}$;

(iii) continuity of H_y, which using (2.3) yields $\partial_z B_z|_{0^+}/\mu_0 = \partial_z H_z|_{0^-} + (\mu_r'/\mu_r)H_x|_{0^-}$;

(iv) continuity of the y-component of the electrical field

$$\partial_z H_x|_{0^-} - \partial_x H_z|_{0^-} = \frac{1}{\mu_0}(\partial_z B_x|_{0^+} - \partial_x B_z|_{0^+}) + Rm\frac{B_z|_{0^+}}{\mu_0}. \tag{2.6}$$

The last term of this equation is the ω-effect coming from the infinite shear located at $z = 0$. It is proportional to Rm and produces a field in the x-direction from a field in the z-direction.

The induction equation inside the fluid has x-independent coefficients. We use a Fourier decomposition in this direction too to get the solutions

$$\boldsymbol{B}^{(q)} \exp(st + \mathrm{i}ky + \mathrm{i}qx - \sqrt{s + k^2 + q^2 + \mathrm{i}qRm}z), \tag{2.7}$$

where q is the wavenumber in the x-direction. For each Fourier mode in the x-direction, we can thus write

$$\partial_z B_x|_{0^+}^{(q)} = -\sqrt{s + k^2 + q^2 + \mathrm{i}qRm}B_x|_{0^+}^{(q)}, \tag{2.8}$$

$$\partial_z B_z|_{0^+}^{(q)} = -\sqrt{s + k^2 + q^2 + \mathrm{i}qRm}B_z|_{0^+}^{(q)}, \tag{2.9}$$

and combine the four matching relations written above to get two boundary conditions on the field inside the structured boundary

$$\begin{aligned}\partial_z H_x|_{0^-}^{(q)} - \mathrm{i}qH_z|_{0^-}^{(q)} + \sqrt{s + k^2 + q^2 + \mathrm{i}qRm}H_x|_{0^-}^{(q)} + \mathrm{i}q\{\mu_r H_z|_{0^-}\}^{(q)} \\ - Rm\{\mu_r H_z|_{0^-}\}^{(q)} = 0\end{aligned}, \tag{2.10}$$

$$\partial_z H_z|_{0^-}^{(q)} + \left\{\frac{\mu_r'}{\mu_r}H_x|_{0^-}\right\}^{(q)} + \sqrt{s + k^2 + q^2 + \mathrm{i}qRm}\{\mu_r H_z|_{0^-}\}^{(q)} = 0, \tag{2.11}$$

where $\{F\}^{(q)}$ is the amplitude of field F on the Fourier mode $\mathrm{e}^{\mathrm{i}qx}$. Note that the Fourier modes are coupled: as μ_r is x-dependent, a term like $\{\mu_r H_z|_{0^-}\}^{(q)}$ involves the Fourier amplitudes $q - 1$ and $q + 1$ of $H_z|_{0^-}$. The system (2.4)–(2.5) to be solved involves two equations coupling two real-valued fields. These equations are second-order in z. Accordingly, we have two complex boundary conditions at $z = 0$ and two at $z = -D$, which correspond to eight real boundary conditions.

3. Numerical calculation of the onset of linear instability

Solving the kinematic dynamo problem consists of computing the allowed values of s. One then seeks a critical value of Rm for which the real part of s vanishes. This task is performed using a numerical code which is spectral in the x-direction and uses finite differences in z. More information on this code is given in appendix A. Let us first focus on the harmonic response of the system, i.e. we seek a solution with the same spatial period in the x-direction as the permeability modulation, the possibility of a subharmonic response being discussed in the next section.

3.1. *Dynamo induced by the magnetic permeability modulation*

The first result is that there is a dynamo: provided Rm is high enough, the magnetic permeability modulation together with the flow destabilizes a magnetic mode. Modulating the magnetic permeability of the boundary is thus a way to bypass the anti-dynamo theorem for planar velocity fields (see discussion in § 7.2).

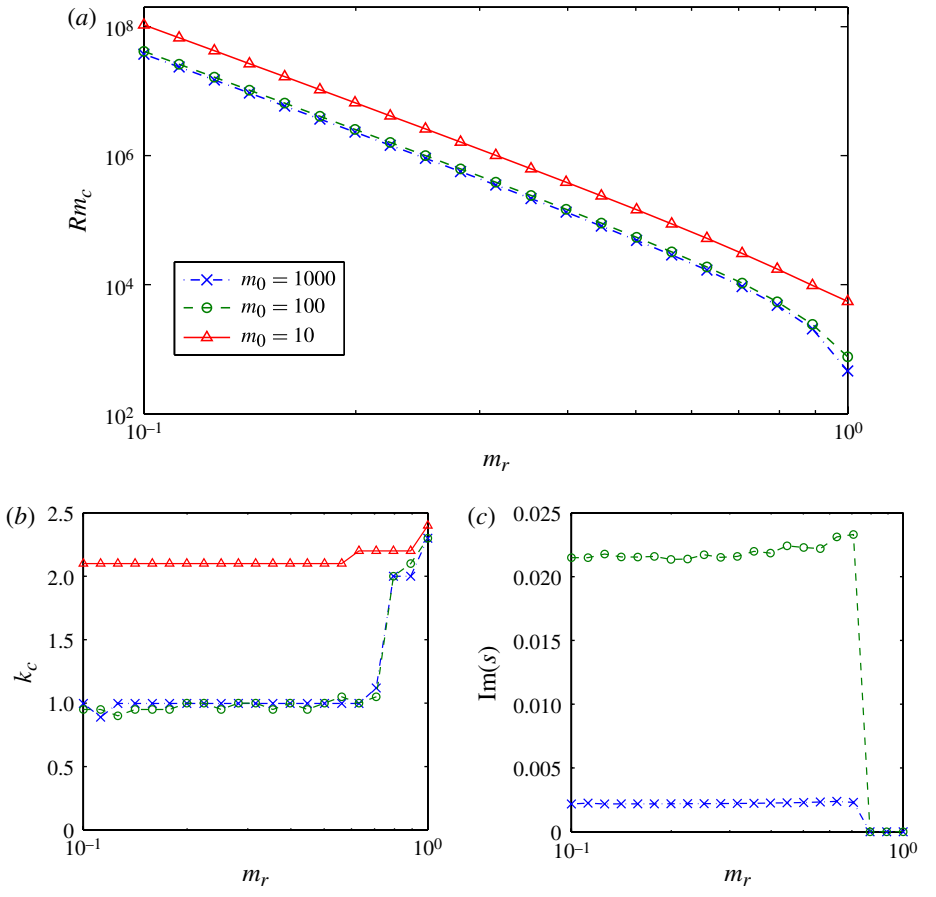

FIGURE 2. (Colour online) (*a*) Critical magnetic Reynolds number, (*b*) wavevector and (*c*) angular frequency at criticality, as a function of the relative magnetic permeability modulation, for $D = 1$. For $m_0 = 10$ the most unstable mode is stationary. For $m_0 = 100$ and $m_0 = 1000$, the Rm_c and k_c curves almost lie on top of each other, which indicates the existence of a limiting curve as m_0 becomes large. The frequency at onset drops by a factor of ten when m_0 increases from 100 to 1000.

We plot in figure 2 the critical magnetic Reynolds number, the wavenumber k_c and the angular frequency $\mathrm{Im}(s)$ at criticality, as a function of the relative permeability modulation $m_r = m_1/(m_0 - 1)$. We assume that the boundary is nowhere diamagnetic, so that μ_r is everywhere higher than one. The quantity m_r is always between 0 and 1, whatever the value of m_0. Zero permeability modulation gives $m_r = 0$, while a maximum permeability modulation $\mu_r(x) = m_0 + (m_0 - 1)\sin x$ corresponds to $m_r = 1$. The computations are performed for $D = 1$. The stronger the permeability modulation, the lower the dynamo onset. As this modulation goes to zero, the critical Rm diverges in agreement with an anti-dynamo theorem valid for zero modulation. This divergence scales as m_r^{-4}.

The first unstable eigenmode is stationary for $m_0 = 10$. For m_0 large ($m_0 = 100$, 1000), it is oscillatory provided that the modulation is weak enough, and it becomes stationary for strong modulation (m_r of order unity). When m_0 is increased from 100

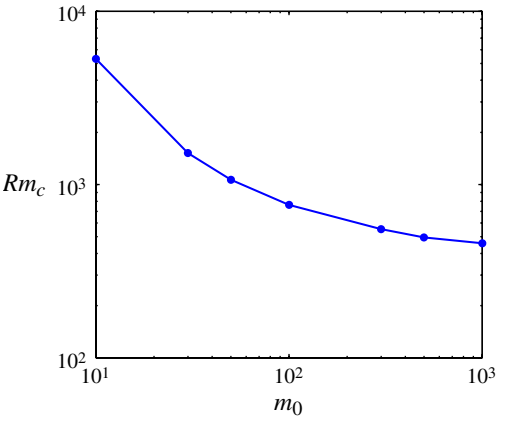

FIGURE 3. (Colour online) Critical magnetic Reynolds number as a function of m_0 for $D = 1$ and a magnetic permeability $\mu_r(x) = m_0 + (m_0 - 1)\sin x$. The dynamo is stationary. The wavenumber of the most unstable mode varies, but remains in the range $k_c = 2.3 \pm 0.1$.

to 1000, the dynamo threshold as well as the value of m_r for transition between stationary and oscillatory dynamos is roughly unchanged. However, we observe that the angular frequency of the oscillatory mode decreases by a factor 10. It is almost independent of m_r and is of order of $1/m_0$. In dimensional units, it is thus of the order of an inverse diffusive time scale based on the spatially averaged magnetic permeability.

Finally, for a fixed value of m_r and high values of m_0, the dynamo onset is a decreasing function of m_0 which tends to a finite limit as $m_0 \to \infty$. We show in figure 3 the onset of stationary dynamo as a function of m_0 for $m_1 = m_0 - 1$ (maximum modulation of μ_r, corresponding to $m_r = 1$) and $D = 1$. The onset is still minimized with respect to the wavenumber k. This minimum value is obtained around $k = 2.3$ for the parameter values of this figure. Within 5% accuracy, the critical magnetic Reynolds number is 5483 for $m_0 = 10$, 763 for $m_0 = 100$, and 458 for $m_0 = 1000$.

3.2. *Influence of the thickness D of the modulated boundary*

We plot in figure 4 the critical magnetic Reynolds number Rm_c and wavenumber at criticality k_c as a function of the thickness D of the boundary. Rm_c decreases to a finite value in the limit of large D. It diverges as D^{-1} when D goes to zero. This divergence traces back to the magnetic field gradients being stronger: at low values of D the characteristic scale of the eigenmode in the y-direction is the thickness of the boundary. We also note that if D is large enough compared to L, the first unstable mode is stationary.

The bifurcation structure observed in the parameter space of the system is thus quite rich. The transition between stationary and oscillatory modes close to the codimension-two bifurcation point and the symmetries broken by the bifurcated solutions are studied below. In § 5 we describe in detail the different regimes observed in the parameter space, using an asymptotic expansion valid for weak permeability modulation.

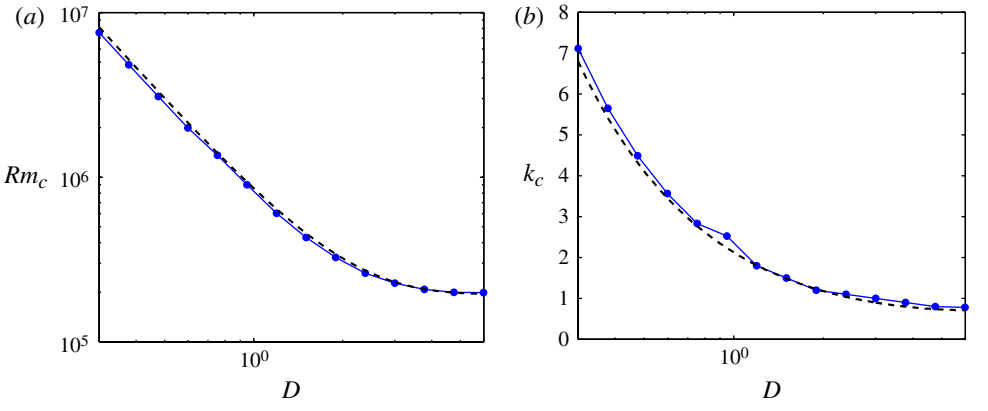

FIGURE 4. (Colour online) (*a*) Magnetic Reynolds number and (*b*) wavenumber at criticality as a function of the thickness of the modulated boundary, for $m_0 = 10$ and $m_1 = 3$ ($m_r = 1/3$). Solid lines with circles are from the numerical computation, and dashed lines come from the asymptotic expansion for weak permeability modulation presented in § 5.

4. Structure and dynamics of the eigenmode

4.1. *High-permeability regions channel the magnetic field*

The eigenmode inside the boundary is shown in figure 5 for $m_0 = 10$ and $m_r = 1$. The field $\boldsymbol{H}$ is localized where the magnetic permeability is the lowest. It has sharp variations in x close to the minimum of μ_r, which is located at $x = 3\pi/2$. This localization of $\boldsymbol{H}$ gets stronger when m_0 increases (with still $m_1 = m_0 - 1$). As a consequence the numerical resolution needed to perform the computation increases strongly when m_0 goes from 10 to 1000. By contrast, the field $\boldsymbol{B}$ has variations much smoother than $\boldsymbol{H}$ in the x-direction.

The field has a non-zero x-averaged component. Outside the modulated boundary this large-scale field is mostly along the x-direction. This traces back to the high value of Rm_c, which corresponds to a strong ω-effect that converts a tiny field along z into a strong field along x. An x-dependent field is superposed on this large-scale field. It is localized close to the boundary $z = 0$ and decreases very rapidly as z increases. Away from the boundary, one sees mostly a field along x and independent of x. Close to $z = 0$, the regions of large magnetic permeability strongly bend the magnetic field: the field lines of $\boldsymbol{B}$ cross the boundary $z = 0$ in such a way that they are in the high-permeability regions for $z < 0$.

4.2. *Competition between stationary and oscillatory eigenmodes*

We showed in figure 2 a transition from oscillatory to stationary dynamo when m_r increases for large m_0, with a discontinuous jump in wavenumber and frequency at onset. To shed some light on this transition, we plot in figure 6 the growth rate $\mathrm{Re}(s)$ of the least stable mode as a function of k, for $m_0 = 100$, $Rm = 10000$, and several values of m_r. This graph shows how the stationary and oscillatory eigenmodes are related: as k decreases from large values, two stationary eigenvalues collide to produce two complex-conjugate eigenvalues, with imaginary parts proportional to the square root of the distance from the collision point. Such collision points are ubiquitous in stability analyses. They originate from the determinant of the linear system having

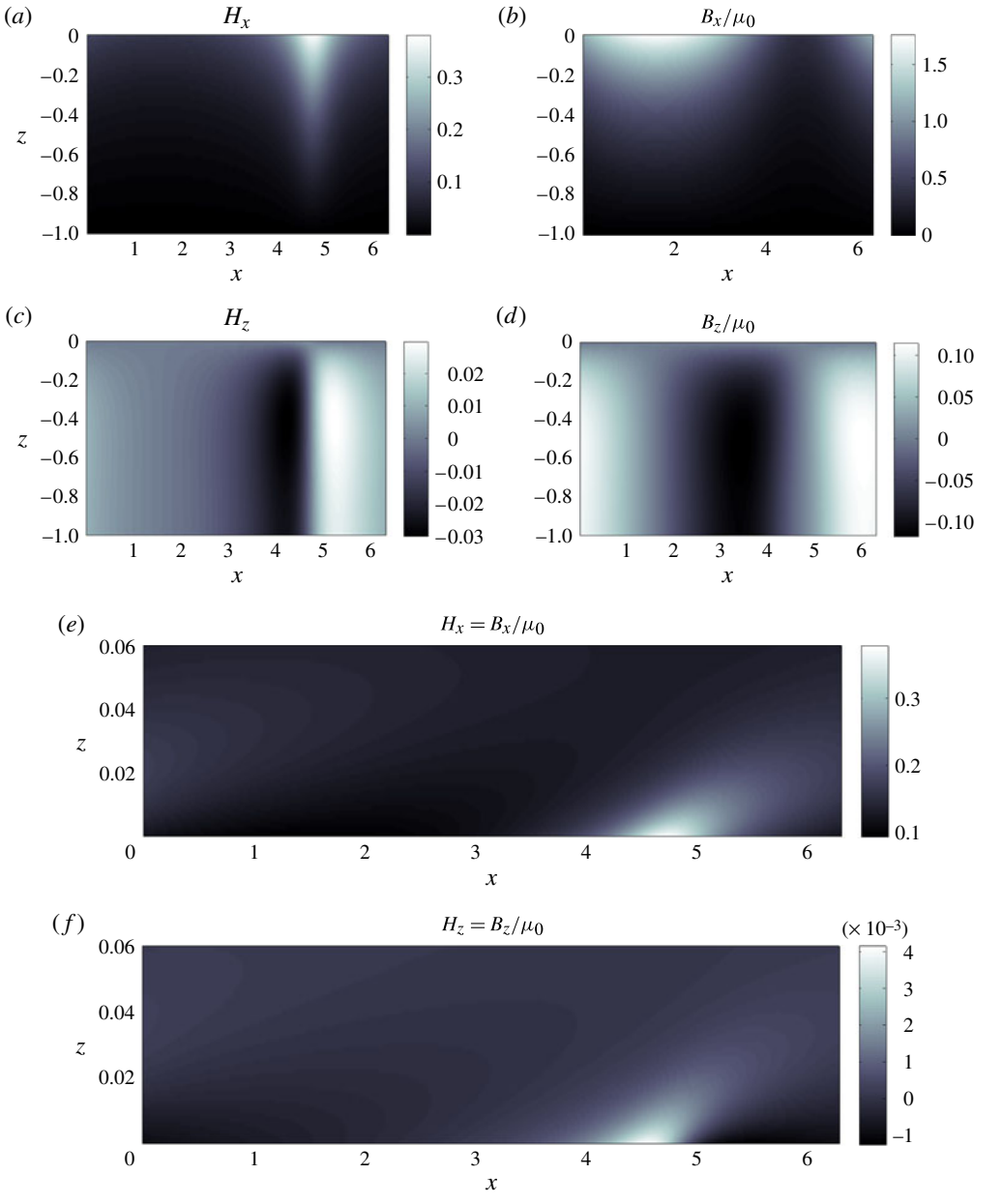

FIGURE 5. (Colour online) Neutral mode of the magnetic field for $m_0 = 10$, $m_1 = 9$ ($m_r = 1$), $D = 1$. The wavenumber at criticality is $k_c = 2.3$ and the magnetic Reynolds number is $Rm_c = 5483$. Frames (*a–d*) correspond to the field inside the boundary, while (*e*) and (*f*) show the field inside the fluid. This field varies harmonically in the y-direction (H_x and H_z in phase, H_y in quadrature). For these parameter values, the field is stationary.

a zero discriminant at the collision point, thus switching from having two real roots (eigenvalues) to two complex-conjugate ones.

From such graphs one can extract the growth rate of the most unstable mode as a function of m_r. We compute it by maximization over k. As can be seen in figure 7,

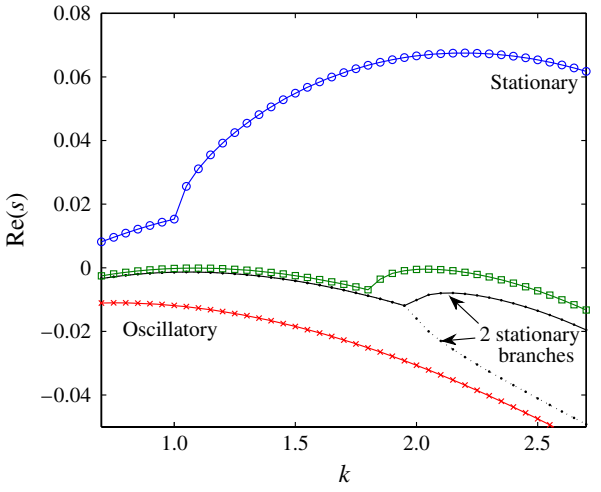

FIGURE 6. (Colour online) Growth rate of the least stable mode as a function of k, for $Rm = 10\,000$, $m_0 = 100$, $D = 1$, and several values of m_r: $\times$, $m_r = 0.606$, the least stable mode is oscillatory; $\cdot$, $m_r = 0.707$, the oscillatory branch splits into two stationary branches (the lower stationary branch is represented only for this value of m_r); $\square$, $m_r = 0.716$, this is the transition point where the stationary and oscillatory eigenmodes are equally stable; their maximum growth rate is close to zero, the system being near the codimension-two point $(Rm, m_r) = (10\,120, 0.71519)$. $\circ$, $m_r = 0.808$, the most unstable mode is stationary.

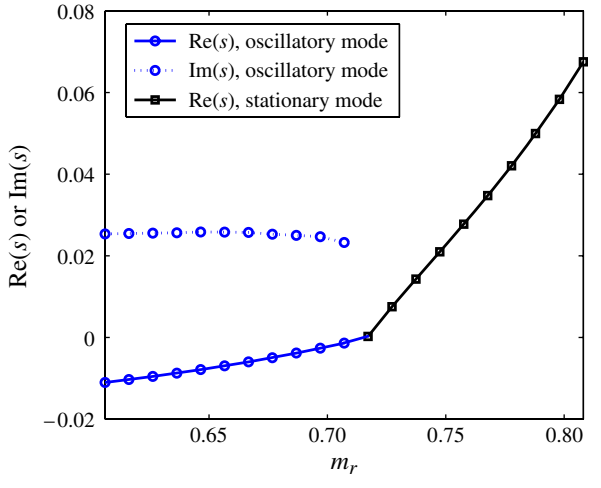

FIGURE 7. (Colour online) Growth rate Re(s) and angular frequency Im(s) of the least stable mode, maximized over k, for $Rm = 10\,000$, $m_0 = 100$ and $D = 1$. The transition from oscillatory to stationary eigenmode occurs for $m_r = 0.716$, with a discontinuous jump in frequency and wavenumber k of the least stable mode. The growth rate at the transition point is negative but very close to zero, the system being near to the codimension-two point $(Rm, m_r) = (10\,120, 0.71519)$.

the most unstable mode is oscillatory for $m_r < 0.716$ and stationary for $m_r > 0.716$. At the transition point $m_r = 0.716$, the system switches from oscillatory to stationary behaviour with finite frequency at the transition, and a jump in y wavenumber. In other words, because the wavenumber k is not a control parameter, the continuous transition between stationary and oscillatory eigenmodes in the constant-m_r curves of figure 6 results in discontinuous jumps in figure 2(*b*,*c*).

The transition point between the oscillatory and stationary eigenmodes in figure 7 corresponds to a very small absolute value of the growth rate of these two modes. This traces back to this transition point being very close to the codimension-two point, where the stationary and oscillatory modes are both neutrally stable for the same parameter values. For $D = 1$ and $m_0 = 100$, the codimension-two point is located at $(Rm, m_r) = (10\,120, 0.71519)$. Note that this codimension-two point differs from the one obtained for a Takens–Bogdanov bifurcation, in the vicinity of which the oscillation frequency continuously goes to zero (Guckenheimer & Holmes 1986). As said above, this results from the selection of a different wavenumber with maximum growth rate in the oscillatory and stationary regimes. This frequently occurs in spatially extended systems, as for instance in the case of thermal convection in a rotating layer studied by Knobloch & Silber (1990).

4.3. *A symmetry-breaking transition*

We plot in figure 8 the lines of (B_x, B_y) in the plane $z = 0^+$, that is the horizontal plane that lies inside the fluid but very close to the modulated boundary. We first observe that the shape of the field lines does not seem to be affected by the flow breaking the $x \to -x$ reflection symmetry. As mentioned by Busse & Wicht (1992) in the case of magnetic field generated by a spatial modulation of electrical conductivity, this is observed when the boundary is thin (here $D = 1$). In the limit of a thick boundary, field lines are more clearly asymmetric, as expected for a system that has no $x \to -x$ reflection symmetry (see Wicht & Busse 1994). In addition, the asymmetry is more apparent in the flow for $z > 0$ as shown in figure 5. Although the velocity field imposes a preferred direction along x, the oscillatory eigenmodes do not propagate along x: they remain 'trapped' by the magnetic permeability modulation, which prevents a drift in the x-direction. By contrast, the problem is invariant under the $y \to -y$ reflection symmetry. We observe that, while the stationary eigenmode is symmetric in y, the oscillatory eigenmodes are not. In the latter case, the $y \to -y$ symmetry is broken by the spatial structure of the mode. This selects the direction of propagation of the field. One oscillatory eigenmode can be obtained from the other one through a reflection in y, therefore these two eigenmodes propagate along y in opposite directions.

4.4. *Subharmonic response*

When discussing the structure and dynamics of the eigenmode, it is important to address the possibility of a subharmonic instability in the system. Indeed, the linear system of equations we are studying has periodic coefficients in the x-direction. So far we have looked only at the harmonic response of this system. However, when a parameter of a differential equation is modulated periodically (in space or time), the system sometimes displays a subharmonic response, the frequency of which is smaller than the forcing frequency.

In the context of a dynamo with space-varying magnetic permeability, one may speculate whether the x modulation of the permeability can destabilize an eigenmode with a spatial period higher than that of the modulation. We should in general allow

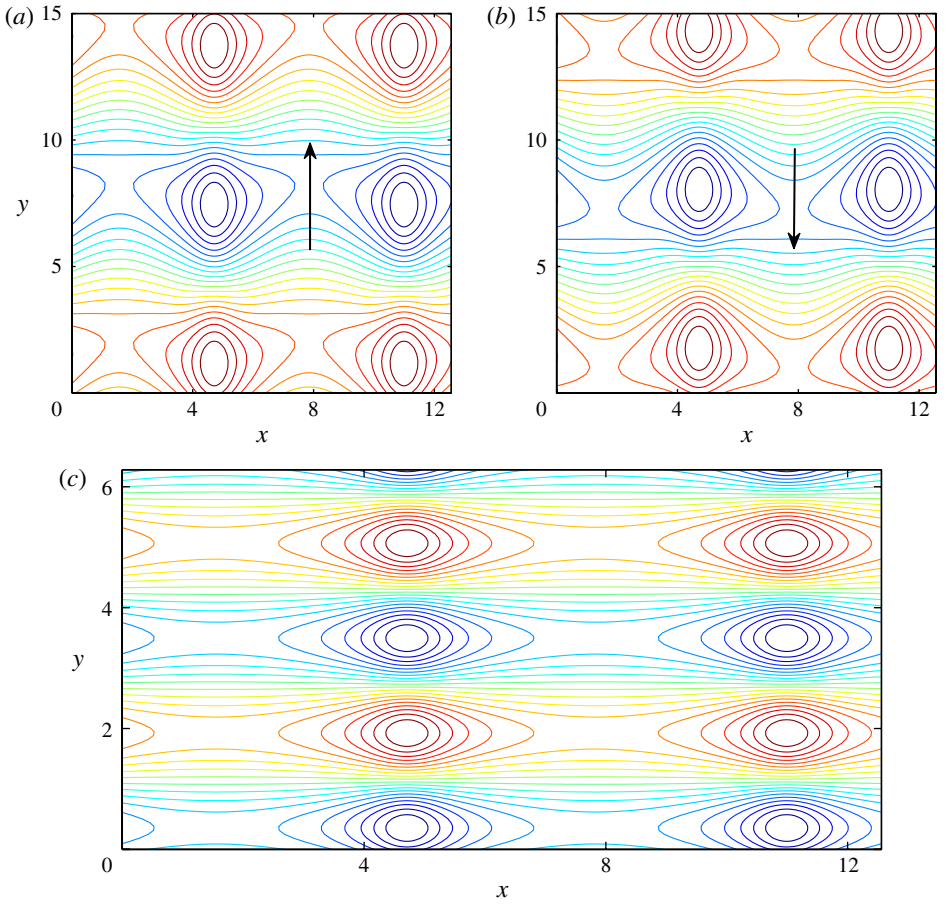

FIGURE 8. (Colour online) Contours of the horizontal magnetic field in the plane $z = 0^+$. (*a,b*) The two oscillatory eigenmodes obtained for $Rm = 10\,000$, $m_0 = 100$, $D = 1$, $m_r = 0.657$ and $k = 0.5$. These eigenmodes break the $y \to -y$ symmetry and therefore propagate along y, in opposite directions. The black arrows indicate the directions of propagation of the eigenmodes. (*c*) Stationary eigenmode computed for $m_r = 0.758$ and $k = 2$, all other parameters being the same. This eigenmode is symmetric to a reflection in y.

for such subharmonic response, and address the problem using Floquet theory. The general solution for (2.4) and (2.5) then reads

$$H_x = \mathrm{e}^{\mathrm{i}Qx}\tilde{H}_x, \tag{4.1}$$

$$H_z = \mathrm{e}^{\mathrm{i}Qx}\tilde{H}_z, \tag{4.2}$$

where the functions $\tilde{H}_x$ and $\tilde{H}_z$ are 2π-periodic in x, and Q is a real number which determines the periodicity of the eigenmode. For instance, $Q = 1/2$ corresponds to the 4π-periodic subharmonic response of the system. The decomposition is inserted into (2.4) and (2.5), which leads to a system of equations for the 2π-periodic functions $\tilde{H}_x$ and $\tilde{H}_z$. We solved these equations numerically, with the parameter Q ranging from 0.1 to 0.5, and we did not find any unstable subharmonic modes, even for very high values of the magnetic Reynolds number. The subharmonic modes are thus much more

stable than the harmonic ones. In the following computations we thus focus on the harmonic response and describe the physical mechanism of the dynamo effect due to spatial modulations of magnetic permeability. This mechanism gives some insight into why subharmonic modes with $Q \in [0.1, 0.5]$ are more stable than harmonic ones. This is discussed in the last section of the paper.

5. Asymptotic expansion for weak-magnetic-permeability modulations

With the goal of shedding light on the mechanism of this dynamo, we now focus on the limit of weak magnetic permeability modulations. Let us write $\mu_r = m_0(1 + \epsilon \sin x)$, with $\epsilon \ll 1$. The relative permeability modulation is $m_r = m_0\epsilon/(m_0 - 1)$. In this limit the x-dependence of the eigenmode is mostly of two kinds:

(i) a large-scale field, i.e. independent of x;

(ii) a harmonic response, that is a field in $\cos x$ and $\sin x$.

The harmonic response is much weaker than the large-scale component: it comes from the effect of the magnetic permeability modulation on the large-scale field, and is thus ϵ times smaller than the latter. We define an average in the x-direction

$$\langle f \rangle = \frac{1}{2\pi} \int_{x-\pi}^{x+\pi} f(\tilde{x})\, \mathrm{d}\tilde{x}, \tag{5.1}$$

and decompose each one of the fields involved in (2.4) and (2.5) into two components

$$H_x = \mathscr{H}_x(z) + h_x(x, z), \tag{5.2}$$

$$H_z = \mathscr{H}_z(z) + h_z(x, z), \tag{5.3}$$

where $\mathscr{H}_x$ and $\mathscr{H}_z$ are the large-scale components and h_x and h_z are the harmonic components. Let us finally assume the ordering $\mathscr{H}_z \ll h_x, h_z \ll \mathscr{H}_x$, with

$$h_x, h_z \sim \epsilon \mathscr{H}_x, \tag{5.4}$$

$$\mathscr{H}_z \sim \epsilon^4 \mathscr{H}_x. \tag{5.5}$$

We will see in what follows that the two quadratures of h_x and h_z (i.e. $\cos x$ and $\sin x$) come at different orders of the asymptotic expansion, and the scaling will be given explicitly only at the last stage of the computation.

5.1. *Coupled evolution of the large-scale and small-scale fields*

Let us divide (2.4) by μ_r^2 before x-averaging it, to get at leading order

$$\partial_{zz}\mathscr{H}_x - (k^2 + m_0 s)\mathscr{H}_x = 0. \tag{5.6}$$

Its solution that satisfies the $z = -D$ boundary conditions is

$$\mathscr{H}_x = \tilde{H}_x \sinh\left(\sqrt{k^2 + m_0 s}(z + D)\right). \tag{5.7}$$

The fluctuating part of the equation gives at dominant order

$$\partial_{zz}h_x - (k^2 + 1 + m_0 s)h_x = \epsilon(1 + m_0 s)\sin(x)\mathscr{H}_x, \tag{5.8}$$

and its solution that satisfies the $z = -D$ boundary conditions is

$$\begin{aligned} h_x = &-\epsilon(1 + m_0 s)\tilde{H}_x \sin(x) \sinh\left(\sqrt{k^2 + m_0 s}(z + D)\right) \\ &+ [a\cos(x) + b\sin(x)] \sinh\left(\sqrt{k^2 + 1 + m_0 s}(z + D)\right). \end{aligned} \tag{5.9}$$

The fluctuating part of (2.5) divided by μ_r yields at leading order

$$\partial_{zz}h_z - (k^2 + 1 + m_0 s)h_z = -\epsilon \cos(x)\partial_z \mathscr{H}_x, \tag{5.10}$$

and its solution that satisfies the $z = -D$ boundary conditions is

$$h_z = \epsilon\sqrt{k^2 + m_0 s}\tilde{H}_x \cos(x)\cosh\left(\sqrt{k^2 + m_0 s}(z + D)\right) + [c\cos(x) + d\sin(x)]\cosh\left(\sqrt{k^2 + 1 + m_0 s}(z + D)\right). \tag{5.11}$$

The x-average of (2.5) divided by μ_r gives finally

$$\partial_{zz}\mathscr{H}_z - (k^2 + m_0 s)\mathscr{H}_z + \langle \epsilon \cos(x)\partial_z h_x\rangle = 0. \tag{5.12}$$

Notice that the two quadratures of h_x scale differently with ϵ: from (5.9), the $\sin x$ quadrature of h_x is of order $\epsilon\mathscr{H}_x$, whereas from (5.12) the $\cos x$ quadrature of h_x is of order $\mathscr{H}_z/\epsilon \sim \epsilon^3\mathscr{H}_x$.

The solution to this equation that is compatible with the boundary conditions at $z = -D$ is

$$\mathscr{H}_z = -\epsilon\frac{a}{2}\sqrt{k^2 + 1 + m_0 s}\cosh\left(\sqrt{k^2 + 1 + m_0 s}(z + D)\right) + \tilde{H}_z\cosh\left(\sqrt{k^2 + m_0 s}(z + D)\right). \tag{5.13}$$

5.2. *Boundary conditions at $z = 0$ and dynamo onset*

The large-scale and small-scale fields are expressed in terms of six real amplitudes $\tilde{H}_x, \tilde{H}_z, a, b, c, d$, so that we need six boundary conditions at $z = 0$. These are obtained by considering the boundary conditions (2.10) and (2.11) for the harmonics $q = 0$ (large-scale field), $q = +1$ and $q = -1$. Details on the computation are given in appendix B. The result is a system of six linear equations with complex coefficients that relate the amplitudes. The complex determinant of this system must vanish for the system to have a non-zero solution. This selects the value of s. At the dynamo onset, the real part of s vanishes and its imaginary part is the angular frequency at onset. Finally, numerical results indicate that the dynamo onset diverges like ϵ^{-4} when ϵ goes to 0. We thus write $Rm = \tilde{Rm}/\epsilon^4$ and expand the determinant of the system to the first non-zero order in ϵ. Imposing that this complex determinant vanishes gives two implicit equations for the critical value of $\tilde{Rm}$ and the frequency at onset.

In what follows, as in the numerical computations presented above, we impose no constraint on the value of k: the system is infinite in the y-direction and perturbations with arbitrary wavelength in y are allowed to develop. We then fix m_0 and D and seek the first mode which becomes unstable as the magnetic Reynolds number increases. With this asymptotic approach we confirm the numerical results presented in figure 2: for a weak modulation of magnetic permeability, we find the same magnetic Reynolds numbers, wavenumbers and frequencies at criticality. More generally, a careful inspection of the parameter space shows that two modes are in competition (and not three modes, as incorrectly stated in Gallet *et al.* 2012).

(i) An oscillatory mode: it is the first unstable mode when D is small and m_0 is large. The wavenumber at onset is of the order of unity for $D = 1$. The frequency of oscillation at onset goes to zero like $1/m_0$ as m_0 increases.

(ii) A stationary mode.

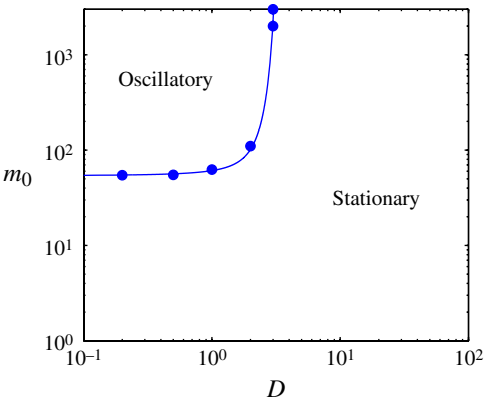

FIGURE 9. (Colour online) Nature of the first unstable mode in the (D, m_0) plane, computed asymptotically for a weak magnetic permeability modulation. Symbols correspond to numerically computed values and the solid line is a guide for the eye.

The stationary or oscillatory nature of the first unstable mode is shown in the (D, m_0) plane in figure 9. Let us recall that this diagram has been computed using an asymptotic expansion and is thus valid for weak magnetic permeability modulations only. For strong enough modulations, we have always observed a stationary first unstable mode (see figure 2).

In the case of a stationary eigenmode, the vanishing determinant yields an analytical expression for the onset

$$\begin{aligned}\sqrt{\tilde{Rm}_c} = &\left[2\sqrt{2}\sinh^2\left(2\sqrt{k^2+1}D\right)(\sinh(kD)+\cosh(kD))(m_0\cosh(kD)+\sinh(kD))\right]\\ &\times\ \Big[4m_0k(k^2+1)\sinh^2(kD)\cosh^4\left(\sqrt{k^2+1}D\right)\\ &-4m_0k^2\sqrt{k^2+1}\sinh(2kD)\sinh\left(\sqrt{k^2+1}D\right)\cosh^3\left(\sqrt{k^2+1}D\right)\\ &+k\left(\cosh^2(kD)\left(m_0k^2\sinh^2\left(2\sqrt{k^2+1}D\right)+4(k^2+1)\sinh^4\left(\sqrt{k^2+1}D\right)\right)\right.\\ &\left.+\ (k^2+1)\sinh^2(kD)\sinh^2\left(2\sqrt{k^2+1}D\right)\right)\\ &-2\sqrt{k^2+1}(2k^2+1)\sinh(2kD)\sinh^3\left(\sqrt{k^2+1}D\right)\cosh\left(\sqrt{k^2+1}D\right)\Big]^{-1},\end{aligned} \tag{5.14}$$

where we assumed $k \geqslant 0$ without loss of generality.

This expression should be considered only where the right-hand side has a positive value, that is for high enough wavenumbers. If $|k|$ is below some value $k_0(D)$ the right-hand side of (5.14) is negative: there is no stationary unstable mode with such low wavenumbers. As k approaches the value $k_0(D)$ from above, the denominator of (5.14) tends to zero and $\tilde{Rm}_c$ diverges. The curve $\tilde{Rm}_c$ as a function of k is drawn in figure 10.

The expression (5.14) is to be minimized with respect to k to find the wavenumber at criticality and the dynamo onset. It has a single minimum. The result of the minimization is shown in figure 4. There is a very good agreement with the numerical computation although $\epsilon = 0.3$ is not particularly small. However, this expression for

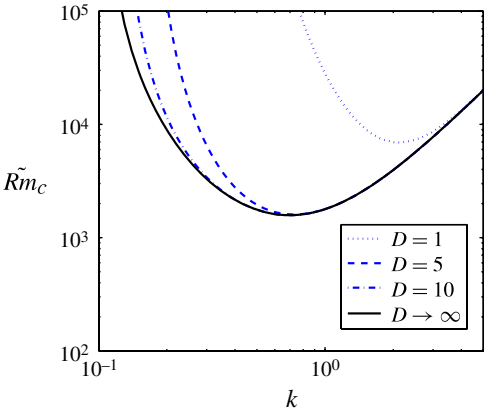

FIGURE 10. (Colour online) $\tilde{Rm}_c$ given by (5.14) as a function of wavenumber k for several values of D. The solid line corresponds to the $D \to \infty$ limit (5.19). $\tilde{Rm}_c$ has a single minimum as a function of k and diverges when k approaches a finite value $k_0(D)$. These plots correspond to $m_0 = 10$.

the onset is quite intricate, and we now wish to consider some limits in which the physics is more easily understood.

5.3. *Onset and structure of the neutral mode for $D \to \infty$*

In the limit of a modulated boundary that occupies the entire half-space $z < 0$, the most unstable mode is stationary ($s = 0$ at onset) and the hyperbolic sines and cosines in z are replaced by exponentials which decrease as $z \to -\infty$. Let us introduce the scalings and write the fields in the following form:

$$\mathscr{H}_x = \hat{H}_x \mathrm{e}^{kz}, \tag{5.15}$$

$$h_x = -\epsilon \hat{H}_x \sin(x)\mathrm{e}^{kz} + (\epsilon^3 \hat{a}\cos(x) + \epsilon \hat{b}\sin(x))\mathrm{e}^{\sqrt{k^2+1}\,z}, \tag{5.16}$$

$$h_z = \epsilon k \hat{H}_x \cos(x)\mathrm{e}^{kz} + (\epsilon \hat{c}\cos(x) + \epsilon^3 \hat{d}\sin(x))\mathrm{e}^{\sqrt{k^2+1}\,z}, \tag{5.17}$$

$$\mathscr{H}_z = -\epsilon^4 \frac{\sqrt{k^2+1}}{2}\hat{a}\mathrm{e}^{\sqrt{k^2+1}\,z} + \epsilon^4 \hat{H}_z \mathrm{e}^{kz}, \tag{5.18}$$

where all the quantities with a hat are of $O(1)$. These quantities satisfy the system of equations written in appendix B, in which the hyperbolic sines and cosines are replaced by 1, and using the substitution $\tilde{H}_x = \hat{H}_x$, $a = \epsilon^3 \hat{a}$, $b = \epsilon \hat{b}$, $c = \epsilon \hat{c}$, $d = \epsilon^3 \hat{d}$, $\tilde{H}_z = \epsilon^4 \hat{H}_z$. The onset of instability is the $D \to \infty$ limit of expression (5.14):

$$\sqrt{\tilde{Rm}_c} = \frac{4\sqrt{2}(1+m_0)}{2k(k^2+1) + m_0 k(2k^2+1) - \sqrt{1+k^2}(1+2k^2+2m_0k^2)}, \tag{5.19}$$

which should be considered only where it is positive, that is for $k > k_0 = (m_0^2 - 1)^{-1/2}$. The threshold has a single minimum value as a function of k:

$$Rm_c = \frac{864}{\epsilon^4}\left(\frac{m_0+1}{m_0-1}\right)^3 \quad \text{for } k_c = \sqrt{\frac{(2+m_0)^2}{3(m_0^2-1)}}. \tag{5.20}$$

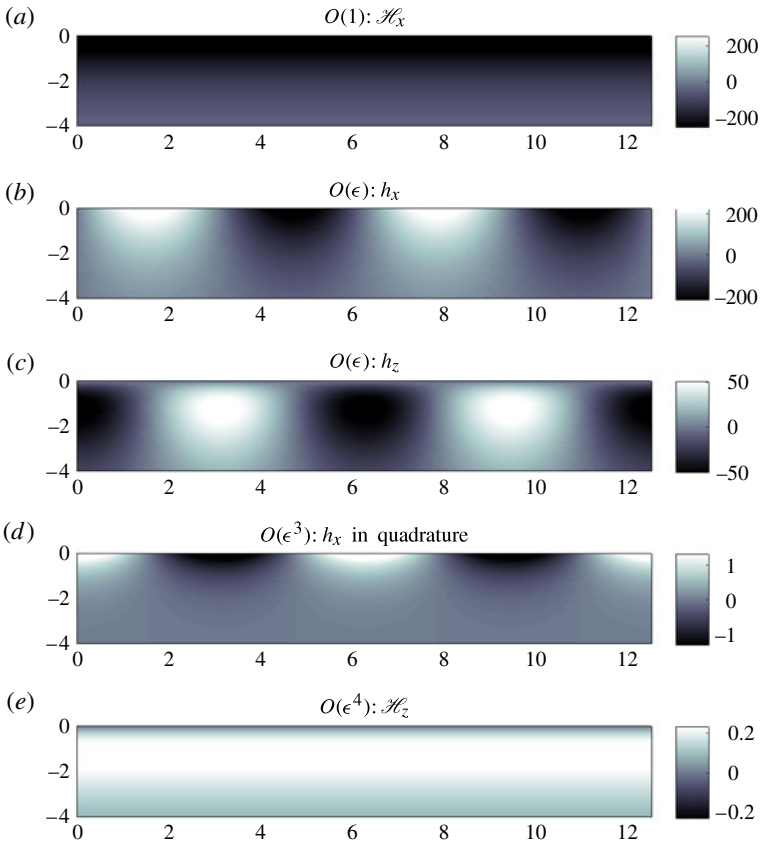

FIGURE 11. (Colour online) Neutral eigenmode in the limit $D \to \infty$ and $m_0 \to \infty$: from the field $\mathscr{H}_x$ (a), the permeability modulation induces an $O(\epsilon)$ component, (b and c), which is advected by the fluid, producing an $O(\epsilon/\sqrt{Rm}) = O(\epsilon^3)$ field (d), which using the permeability modulation once again produces a large-scale field $\mathscr{H}_z$ (e), of $O(\epsilon^2/\sqrt{Rm}) = O(\epsilon^4)$. The shear at $z = 0$ then regenerates the field $\mathscr{H}_x$ through the ω-effect.

For a given and weak relative magnetic permeability modulation m_r, the threshold is thus a decreasing function of the average permeability m_0 of the boundary. Its lowest value is obtained in the limit $m_0 \to \infty$, with

$$k_c = \frac{1}{\sqrt{3}} \quad \text{and} \quad Rm_c = \frac{864}{\epsilon^4}. \tag{5.21}$$

The structure of the neutral mode is quite complicated for arbitrary m_0 but simplifies in this double limit of small ϵ and infinite m_0:

$$\hat{H}_x = -216\sqrt{3}, \quad \hat{a} = \sqrt{3}, \quad \hat{b} = -72\sqrt{3}, \quad \hat{c} = 216, \quad \hat{d} = 0, \quad \hat{H}_z = 1. \tag{5.22}$$

Note that $\hat{d}$ is zero only for infinite m_0.

5.4. *Physical mechanism of this dynamo*

The neutral mode is drawn at each order in figure 11, in the limit of infinite m_0. This plot, together with the scaling laws, sheds some light on the underlying physical mechanism of this dynamo. This mechanism operates in four steps.

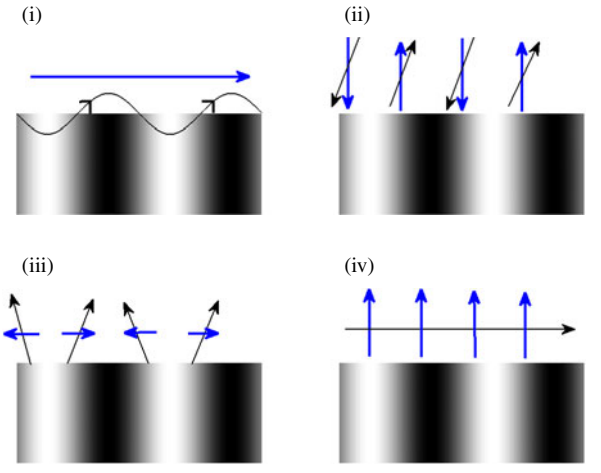

FIGURE 12. (Colour online) Sketch of the effects involved in the dynamo process. At steps (i) and (iii), the tangential component (thick arrow) is converted into a normal one (thin arrow) by the modulation of magnetic permeability in the boundary. At steps (ii) and (iv), the normal component (thick arrow) created at the former step is converted into a tangential one (thin arrow) by the shear. In the boundary, white colour stands for large magnetic permeability.

(i) Let us assume that there is a large-scale field $\mathscr{H}_x$ inside the boundary: the modulation of μ_r creates a small-scale field of order $h_1 \sim \epsilon \mathscr{H}_x$. However, another action of the permeability modulation on h_1 cannot produce a large-scale field $\mathscr{H}_z$: the terms to be averaged are products of quantities oscillating in quadrature and the small scales do not act on the large ones. This traces back to the following symmetry: without the flow, the system is invariant to a reflection about the plane $x = \pi/2$ (for instance). The magnetic field is either even or odd under this transformation, and thus the large-scale field cannot have both an x- and a z-component. One thus has to invoke the flow which breaks the symmetry $x \to -x$, in the step of conversion of $\mathscr{H}_x$ into $\mathscr{H}_z$.

(ii) For the small scales to produce large-scale field, one needs to create some field in quadrature with h_1. This is done through advection by the flow. At the $z = 0$ boundary, the boundary condition (2.11) gives approximately $\sqrt{Rm}h_2 \sim h_1$, hence $h_2 \sim Rm^{-1/2}h_1$. This scaling law corresponds to the skin effect: in a frame travelling with the fluid at velocity $U\boldsymbol{e}_x$, the field that comes out of the boundary is an oscillating field that penetrates into the fluid only in a skin layer of depth of order $Rm^{-1/2}$.

(iii) The field h_2 interacts once again with the permeability modulation to produce a large-scale field $\mathscr{H}_z \sim \langle h_2 \mu_r \rangle \sim \epsilon h_2$.

(iv) Finally, this field $\mathscr{H}_z$ is sheared, which generates large-scale field along x through the ω-effect: $\mathscr{H}_x \sim Rm\mathscr{H}_z$.

These successive steps can be written as a cycle: $\mathscr{H}_x \sim Rm\mathscr{H}_z \sim Rm\epsilon h_2 \sim \sqrt{Rm}\epsilon h_1 \sim \sqrt{Rm}\epsilon^2 \mathscr{H}_x$. At onset, the gain of this cycle is of the order of unity. This gives $Rm \sim \epsilon^{-4}$, in agreement with the results presented above.

The four steps of the mechanism are sketched in figure 12: a magnetic field line along the modulated boundary is channelled by the large-permeability regions to

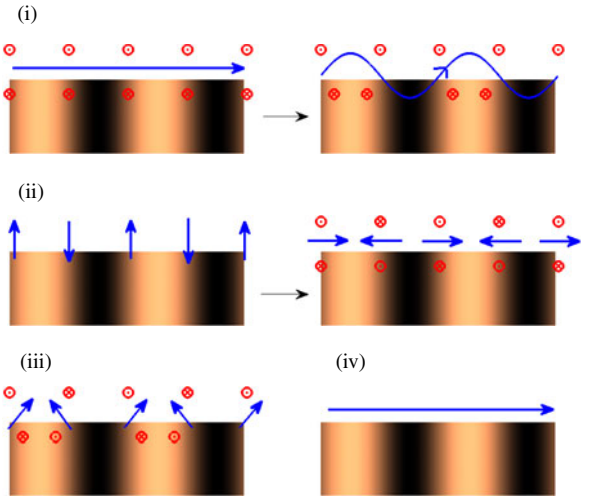

FIGURE 13. (Colour online) Dynamo mechanism for a weak electrical conductivity modulation. In-plane vectors are magnetic field (thick arrows), and vectors perpendicular to the plane are electrical currents (circles with dots or crosses). At steps (i) and (iii), loops of electrical current are channelled by the high conductivity regions, which produces vertical magnetic field. At steps (ii) and (iv), the flow shears the normal magnetic field into field parallel to the boundary. Inside the boundary, light colour stands for large electrical conductivity.

produce small-scale field perpendicular to the boundary (step i). At step (ii), this small-scale field is sheared by the flow, which induces small-scale field parallel to the boundary. This latter is again channelled by the large-μ_r regions and large-scale field perpendicular to the boundary is produced. The ω-effect due to the shear converts this normal field back into a large-scale field parallel to the boundary (step iv).

5.5. *Modulation of electrical conductivity*

A similar mechanism can be invoked to explain the dynamo effect reported by Busse & Wicht (1992), replacing the permeability modulation by a modulation of electrical conductivity, with regions of large electrical conductivity channelling electrical currents. The proposed mechanism is sketched in figure 13. It proceeds in four steps.

(i) Start with a large-scale magnetic field along x. This field depends upon y sinusoidally (it is a Fourier mode in y) and is therefore associated with loops of electrical current contained in y–z planes. Because regions of high electrical conductivity channel electrical currents, these loops are tilted by the conductivity modulation, which produces a small-scale field in the z-direction.

(ii) The shear flow converts the small-scale vertical field into a small-scale horizontal field.

(iii) This small-scale horizontal field is associated with loops of electrical current, alternating in sign along x. Regions of large electrical conductivity channel electrical currents and these loops get tilted. This produces large-scale (i.e. x-independent) magnetic field along z.

(iv) This large-scale field is sheared by the flow, producing large-scale field along x.

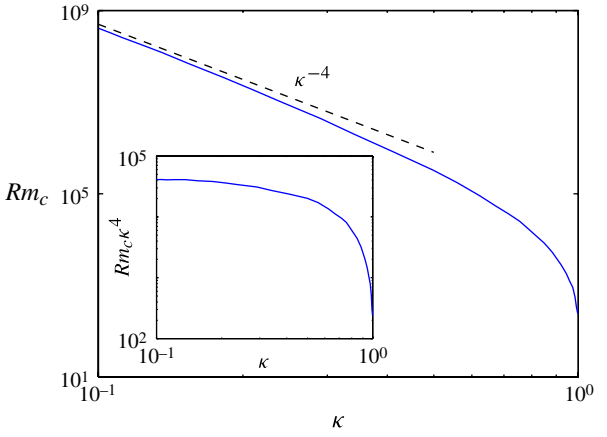

FIGURE 14. (Colour online) Critical magnetic Reynolds number for dynamo action due to spatial modulation of electrical conductivity (data from Busse & Wicht 1992). The thickness of the modulated boundary is $D = 0.1$ and the wavenumber in the y-direction is fixed at $k = 1$. The dashed line indicates the scaling law predicted for low modulation. Inset: critical magnetic Reynolds number compensated by the κ^{-4} scaling predicted for low conductivity modulation.

This mechanism leads to the same scaling law for the dynamo threshold as with a magnetic permeability modulation, $Rm_c \sim \epsilon^{-4}$, where ϵ is now the amplitude of the electrical conductivity modulation. This prediction for the critical magnetic Reynolds number is in agreement with the results of Busse & Wicht (1992). Indeed, their computation corresponds to a setup similar to figure 1, in which the boundary has constant magnetic permeability μ_0 and modulated electrical resisitivity $\sigma^{-1}[1 + \kappa \sin(x/L)]$. Still denoting the magnetic Reynolds number as $Rm = \mu_0 \sigma UL$, Busse & Wicht's results for the threshold of dynamo action translate into an Rm_c versus κ curve for the critical magnetic Reynolds number for steady dynamo action. This curve is shown in figure 14 using data from their paper. It displays an $Rm_c \sim \kappa^{-4}$ scaling regime for low-resisitivity modulation, in agreement with the mechanism described above.

From a comparison of the second snapshots of figures 12 and 13, we note that the permeability and conductivity modulations create harmonic components that have opposite signs for a given sign of the large-scale field, and a given phase of the modulation (for instance when its amplitude vanishes, going from positive to negative values). Provided the qualitative arguments given above remain valid in a system where both the permeability and the conductivity are modulated, a larger effect is expected if the two modulations have opposite amplitudes, that is if a large- (resp. low-) permeability region corresponds to a low- (resp. large-) conductivity region.

6. Relevance of this mechanism to experimental dynamos

We have demonstrated that a spatial modulation of magnetic permeability can generate a dynamo field from a flow which would not be a dynamo in the absence of modulation (whatever the value of the magnetic Reynolds number). However, in the geometry described above this mechanism is not very effective and leads to critical values of Rm hardly achievable in the laboratory. For a strong permeability modulation and m_0 of about 100, the critical magnetic Reynolds number is of order 10^3. For

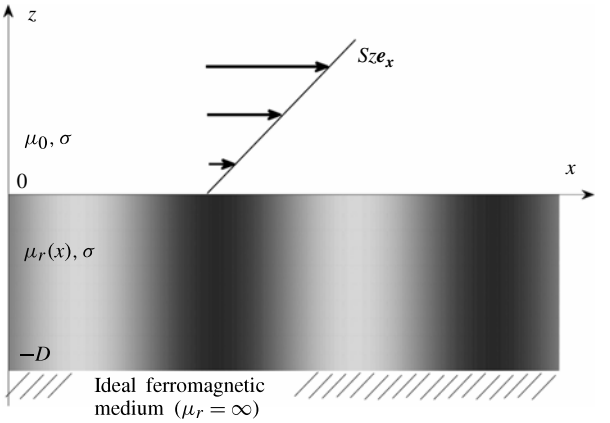

FIGURE 15. An alternative model: we consider a finite and uniform shear inside an electrically conducting fluid, under which is a boundary of spatially modulated magnetic permeability.

a liquid sodium experiment with characteristic size of tens of centimetres, this corresponds to a critical velocity for the fluid of the order of 1 km s^{-1}, which cannot be achieved in the laboratory.

This mechanism in the present state thus seems irrelevant for the VKS experiment. However, we will now see that slight modifications of the system make it a much more efficient dynamo, with critical Rm achievable in a laboratory experiment.

6.1. *Finite shear at* $z = 0$

In the results reported in §§ 3 and 4, infinite shear is localized at $z = 0$. The high dynamo onsets correspond to a very thin skin layer, scaling like $Rm_c^{-1/2}$. In an actual experimental device, the width of the shear layer may not be much thinner than this skin layer. Let us consider then the opposite situation in which the shear extends up to infinity. We will see that this modification leads to larger skin depths and small dynamo thresholds. To wit, we consider the velocity field $\boldsymbol{u} = (Sz, 0, 0)$ sketched in figure 15. The magnetic Reynolds number is now defined using the shear amplitude: $Rm = \mu_0 \sigma S L^2$. For a Fourier mode $\boldsymbol{B}(z)\mathrm{e}^{st+\mathrm{i}qx+\mathrm{i}ky}$ the induction equation inside the fluid reads

$$d_{zz}B_z - (s + q^2 + k^2 + \mathrm{i}qRmz)B_z = 0, \tag{6.1}$$

$$d_{zz}B_x - (s + q^2 + k^2 + \mathrm{i}qRmz)B_x = -RmB_z. \tag{6.2}$$

The solution that tends to zero for z going to infinity is

$$B_x^{(q)} = -a_q \frac{Rm^{1/3}}{(\mathrm{i}q)^{2/3}} \mathrm{Ai}'(F_q(z)) + b_q \mathrm{Ai}(F_q(z)), \tag{6.3}$$

$$B_z^{(q)} = a_q \mathrm{Ai}(F_q(z)), \tag{6.4}$$

where Ai are Ai' denote respectively the Airy function and its first derivative, and

$$F_q(z) = \frac{s + k^2 + q^2 + \mathrm{i}qRmz}{(\mathrm{i}qRm)^{2/3}}. \tag{6.5}$$

The above solution is valid only for $q \neq 0$. The $q = 0$ Fourier mode must be dealt with separately and leads to the solution

$$B_x^{(0)} = \frac{a_0 Rm}{2\sqrt{s+k^2}} z \exp\left(-\sqrt{s+k^2}\, z\right) + b_0 \exp\left(-\sqrt{s+k^2}\, z\right) \tag{6.6}$$

$$B_z^{(0)} = a_0 \exp\left(-\sqrt{s+k^2}\, z\right). \tag{6.7}$$

In these expressions the coefficients $(a_q)_{q\in\mathscr{Z}}$ and $(b_q)_{q\in\mathscr{Z}}$ are integration constants. After a straightforward calculation, the continuity of B_z, H_x, H_y and the y-component of the electric field leads to two boundary conditions for the field inside the modulated boundary:

$$\begin{aligned}\partial_z H_x|_{0^-}^{(q)} = {} & \mathrm{i}qH_z|_{0^-}^{(q)} - \mathrm{i}q\{\mu_r H_z|_{0^-}\}^{(q)} + (\mathrm{i}qRm)^{1/3}\frac{\mathrm{Ai}'(F_q(0))}{\mathrm{Ai}(F_q(0))}H_x|_{0^-}^{(q)} \\ & - \frac{Rm^{2/3}}{(\mathrm{i}q)^{1/3}}\left(F_q(0) - \frac{(\mathrm{Ai}'(F_q(0)))^2}{(\mathrm{Ai}(F_q(0)))^2}\right)\{\mu_r H_z|_{0^-}\}^{(q)},\end{aligned} \tag{6.8}$$

$$\partial_z H_z|_{0^-}^{(q)} = -\left\{\frac{\mu_r'}{\mu_r}H_x|_{0^-}\right\}^{(q)} + (\mathrm{i}qRm)^{1/3}\frac{\mathrm{Ai}'(F_q(0))}{\mathrm{Ai}(F_q(0))}\{\mu_r H_z|_{0^-}\}^{(q)}, \tag{6.9}$$

for $q \neq 0$, and for $q = 0$:

$$\partial_z H_x|_{0^-}^{(0)} = -\sqrt{s+k^2}H_x|_{0^-}^{(0)} + \frac{Rm}{2\sqrt{s+k^2}}\{\mu_r H_z|_{0^-}\}^{(0)}, \tag{6.10}$$

$$\partial_z H_z|_{0^-}^{(0)} = -\left\{\frac{\mu_r'}{\mu_r}H_x|_{0^-}\right\}^{(0)} - \sqrt{s+k^2}\{\mu_r H_z|_{0^-}\}^{(0)}. \tag{6.11}$$

These new boundary conditions replace (2.10) and (2.11) when assuming a finite shear that extends up to infinity.

6.2. *A much more efficient dynamo*

We display in figure 16 the critical magnetic Reynolds number of the finite-shear dynamo. The onset is much lower than for an infinite shear located at $z = 0$. More interestingly, at small modulation ϵ the onset diverges as $Rm_c \sim \epsilon^{-3}$. The exponent of divergence thus goes from -4 to -3 when one considers a finite shear instead of an infinite shear located at $z = 0$. This traces back to a modification of the skin depth in the presence of finite shear. The argument (6.5) of the Airy functions scales at large z like $Rm^{1/3}z$. Hence the skin depth no longer scales as $Rm^{-1/2}$, but as $Rm^{-1/3}$: the magnetic field penetrates deeper into the fluid and advection is enhanced. Coming back to the previously discussed mechanism, step (ii) becomes $h_2 \sim Rm^{-1/3}h_1$, so that the cycle reads $\mathscr{H}_x \sim Rm\mathscr{H}_z \sim Rm\epsilon h_2 \sim Rm^{2/3}\epsilon h_1 \sim Rm^{2/3}\epsilon^2\mathscr{H}_x$. The onset is obtained when the gain of this cycle is of the order of unity, which gives $Rm_c \sim \epsilon^{-3}$. Finally, we mention that this dynamo is oscillatory at onset, with an angular frequency ranging from 0.14 at low modulation to 0.25 at maximum modulation. It corresponds to a travelling wave in the y-direction.

Such a modification of the skin depth also occurs in the Ponomarenko dynamo when one considers a smooth velocity profile instead of a discontinuous one (Gilbert 1988): if the velocity field has a finite-amplitude jump, the eigenmodes develop on a characteristic scale $Rm^{-1/2}$ in the radial, azimuthal and axial directions, whereas for a smooth velocity profile this characteristic scale is $Rm^{-1/3}$.

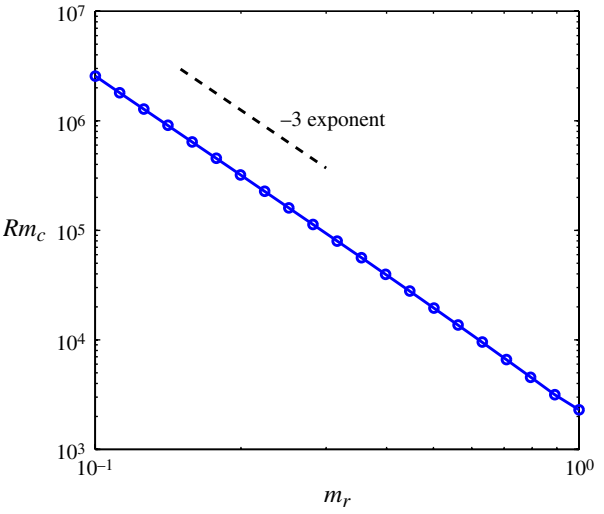

FIGURE 16. (Colour online) Onset of dynamo action computed for a finite shear inside the fluid, $m_0 = 10$ and $D = 1.0$. The wavenumber at criticality has little dependence on m_r and is close to 0.6. Pulsation at onset ranges between 0.14 for weak modulation and 0.25 for maximum modulation.

6.3. *Influence of the thickness D*

The onset, wavenumber and angular frequency at criticality are plotted in figure 17 as a function of the thickness D of the modulated boundary; m_0 is either 10 or 100, the modulation being fixed to its maximum value $m_1 = m_0 - 1$. The onset is a rapidly decreasing function of D which saturates for large D. For $m_0 = 100$ the critical magnetic Reynolds number becomes as low as 15. The dynamo is oscillatory and would correspond in the VKS experiment to a wave travelling in the radial direction. However, the frequency at onset goes to zero as m_0 and/or D increase, so that switching from Cartesian to cylindrical geometry might be sufficient to make this dynamo stationary.

This mechanism is the first to suggest a determining role of the VKS impeller ferromagnetic blades in the magnetic field generating process. However, using the definition $Rm = \mu_0 \sigma S L^2$, where $2\pi L$ is the distance between the blades, gives small values of the magnetic Reynolds number in the VKS experiment. Indeed, if we assume that the azimuthal velocity close to the disks decays on an axial length equal to the blade height (41 mm), the shear for a rotation frequency of 25 Hz is approximately $S = 600\ \mathrm{s}^{-1}$. Using $L \simeq 2$ cm for the VKS experiment gives a maximum magnetic Reynolds number of 3. This is smaller than any value of dynamo threshold reported in this study. A better description of the geometry and velocity field of the VKS experiment would be necessary for further comparison, and to quantify the conversion of toroidal to poloidal magnetic field induced by the ferromagnetic blades. In the following section, we focus on the role of the disk to which these blades are attached.

6.4. *Role of the ferromagnetic disk*

With the goal of studying the role of the ferromagnetic disk on which the blades are attached, we consider the situation in which the medium at $z < -D$ is an insulator with magnetic permeability μ_0. Inside the insulator the Laplacian of the magnetic field

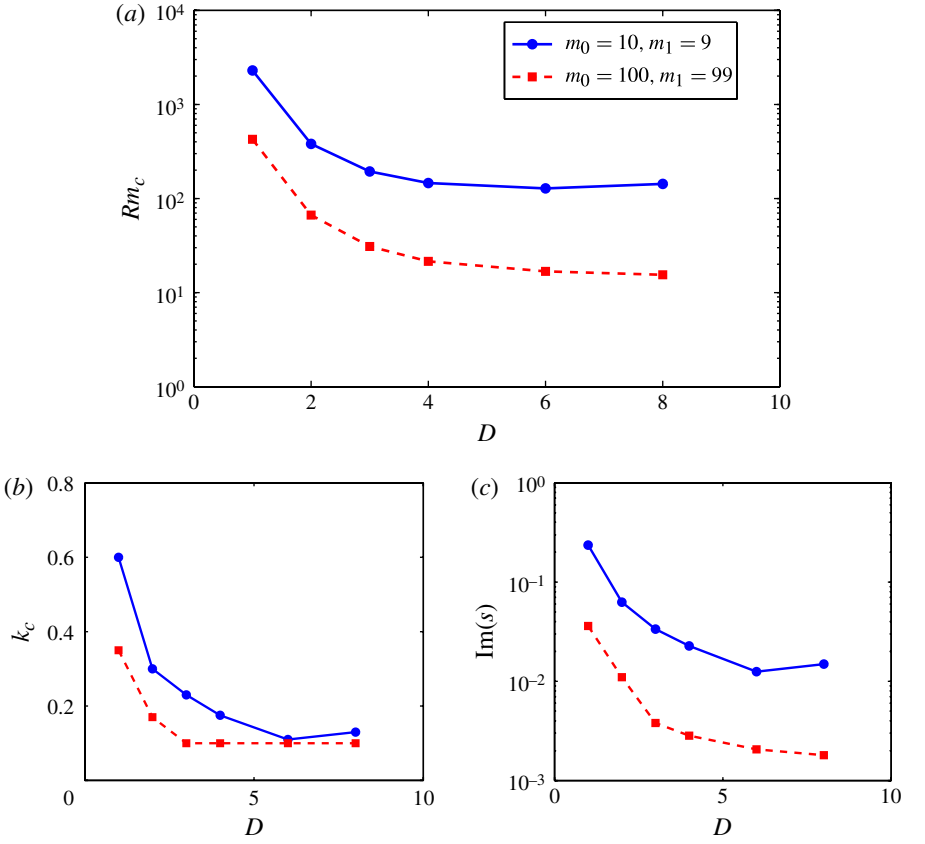

FIGURE 17. (Colour online) (*a*) Dynamo onset, (*b*) wavenumber and (*c*) angular frequency at criticality as a function of the thickness D of the modulated boundary, for a uniform shear flow. For $m_0 = 100$ and large enough D, the critical Rm reaches values of the order of 15.

vanishes. A Fourier mode of wavevectors q and k respectively in x and y thus has the z-dependence $\exp(\sqrt{q^2+k^2}\,z)$. This solution is the one that vanishes as z goes to $-\infty$. Making use of the continuity of B_z, H_x and H_y, one can derive the following boundary condition at $z=-D$ for the field inside the boundary:

$$\left\{\frac{\mu_r'}{\mu_r}H_x|_{-D^+}\right\}^{(q)} + \partial_z H_z|^{(q)}_{-D^+} = \sqrt{k^2+q^2}\{\mu_r H_z|_{-D^+}\}^{(q)}. \tag{6.12}$$

Setting to zero the normal component of the electric field at the insulator boundary gives the second boundary condition

$$H_x|^{(q)}_{-D^+} = \frac{\mathrm{i}q}{\sqrt{q^2+k^2}}\{\mu_r H_z|_{-D^+}\}^{(q)}. \tag{6.13}$$

This relation can be used to simplify the first boundary condition and express the z-derivative of H_z at $-D^+$ only in terms of $H_z|_{-D^+}$. The two boundary conditions allow this new eigenvalue problem to be solved.

We compare in figure 18 the dynamo onset obtained for an insulating medium at $z<-D$ to the one obtained for an ideal ferromagnetic material ($\mu_r=\infty$). In order

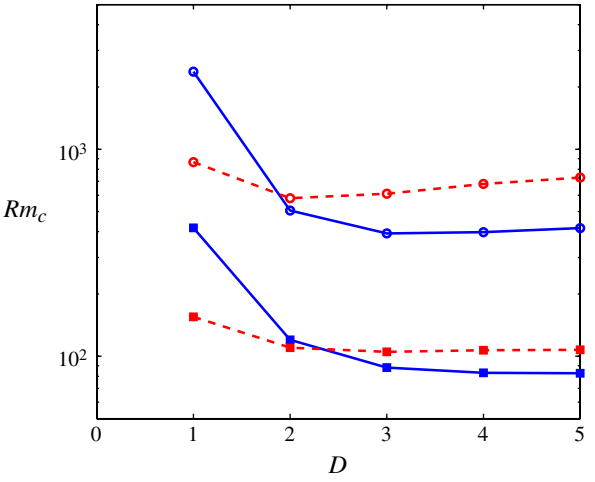

FIGURE 18. (Colour online) Onset of dynamo action: the medium at $z < -D$ is either made of insulating material (dashed line) or of ideal ferromagnetic material ($\mu_r = \infty$, solid line). Circles: $m_0 = 10$ and $m_1 = 9$; squares: $m_0 = 100$ and $m_1 = 99$. The wavevector in the y-direction is fixed to $k = 0.5$. The dynamo is stationary for an insulating medium and oscillatory with very low frequency for an ideal ferromagnetic material.

to make possible some comparisons with the VKS experiment, the wavenumber in y is fixed to $k = 0.5$. This direction would be the radial one in the VKS experiment, and the extension of the eigenmode in this direction is of the order of the disk radius, which is of the order of the distance between two blades. For low values of D the onset is lower with an insulator at $z < -D$, whereas for $D > 2.5$ the dynamo is more efficient with a ferromagnetic medium at $z < -D$. This crossing of the curves traces back to two opposing effects of the ferromagnetic material.

(i) The presence of ferromagnetic material at $z = -D$ imposes $B_x = 0$ at the boundary. If D is small, the field along x cannot be very large inside the modulated boundary and the conversion of this toroidal field into poloidal field is limited.

(ii) The ferromagnetic medium channels the field in the z-direction: the field enters the medium at $z = -D$ and escapes it at an arbitrary x without any cost in terms of Ohmic dissipation. By contrast, for an insulating medium part of the field lines must close inside the modulated boundary, which results in stronger field gradients and enhanced Ohmic dissipation.

To illustrate these effects we compare in figure 19 the fields inside the modulated boundary, computed for $D = 2$ and either an insulating or a ferromagnetic medium at $z < -D$: the magnetic field enters the ferromagnetic medium and escapes it half a spatial period away. The eigenmode is oscillatory with a very low frequency for a ferromagnetic medium, whereas it is stationary for an insulating one.

Note that when the VKS impellers are made of ferromagnetic blades attached to stainless steel disks, no magnetic field is observed at the highest reachable magnetic Reynolds number. A Cartesian equivalent of the VKS experiment would rather correspond to the region $D > 2.5$ of figure 18, so that the trend exhibited in the numerical results is consistent with experimental observations. Nevertheless, the difference between the dynamo thresholds computed for a ferromagnetic and an insulating medium is rather small, and the role of the VKS ferromagnetic disks is

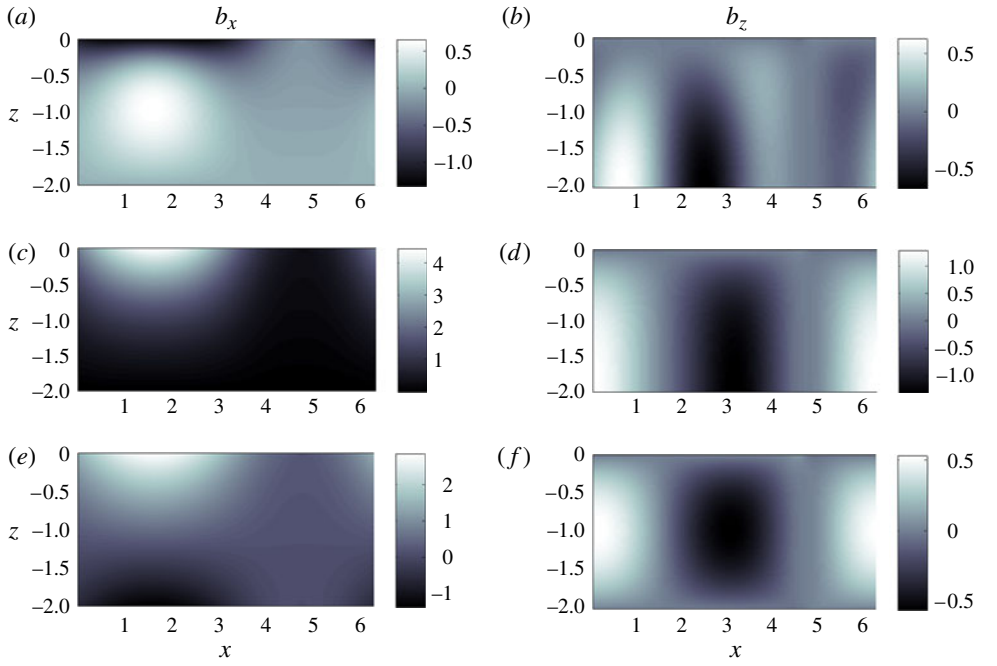

FIGURE 19. (Colour online) Neutral magnetic field mode for $D = 2.0$ and $k = 0.5$: (*a,b*) real part of the eigenmode for a ferromagnetic medium at $z < -D$; (*c,d*) imaginary part of this eigenmode; (*e,f*) eigenmode for an insulating medium at $z < -D$.

likely to be more complex. Indeed, when the VKS disks are counter-rotating, the region behind these disks has an ω-effect whose sign is opposite to the ω-effect between the two disks. This ω-effect is counter-productive and detrimental to the dynamo instability. The ferromagnetic disk thus gives an opportunity for the field to close inside the disk, without having to enter this region of detrimental ω-effect. Such a detrimental effect from 'lid layers' was also reported in numerical simulations (Stefani *et al.* 2006). The flow in the vicinity of the disk is also more complicated than the ones considered here: it has a component parallel to the blades and an azimuthal modulation. The associated helicity is a source of an alpha-effect, put forward as an important mechanism for the VKS dynamo (Pétrélis, Mordant & Fauve 2007). Possible future works concern the investigation of the interplay between the mechanism presented here and other dynamo mechanisms.

7. Discussion

We conclude with an analysis of our results in the framework of spatial symmetries and anti-dynamo theorems.

7.1. *Subharmonic response*

In § 4.4, we presented the subharmonic stability problem with an infinite shear at $z = 0$. We did not find any unstable subharmonic modes with Floquet wavenumber $Q \in [0.1, 0.5]$, even for very high values of the magnetic Reynolds number. These subharmonic modes are thus much more stable than the harmonic ones. This may be explained by the fact that the harmonic response is generically coupled to a

large-scale, x-independent field, whereas the subharmonic response cannot be coupled to such a field. Indeed, let us consider a field ψ having both an x-independent and a subharmonic component

$$\psi(x, z) = \psi_0(z) + \tilde{\psi}_{1/2}(x, z)\mathrm{e}^{\mathrm{i}x/2}, \tag{7.1}$$

where $\tilde{\psi}_{1/2}$ is 2π-periodic in x. The translation $x \to x + 2\pi$ transforms the eigenmode into

$$\psi'(x, z) = \psi_0(z) - \tilde{\psi}_{1/2}(x, z)\mathrm{e}^{\mathrm{i}x/2}. \tag{7.2}$$

This translation leaves the setup invariant and ψ' is thus an eigenmode of the system for the same eigenvalue. Performing the sum and difference of ψ and ψ' leads to the conclusion that the x-independent and subharmonic components decouple.

Therefore the $Q = 1/2$ subharmonic response cannot benefit from the coupling with the large-scale field, which has weak Ohmic dissipation. Indeed, this latter is not subject to a skin effect and thus has a large spatial extension. It is the coupling with this large-scale mode that makes the harmonic response unstable. The absence of coupling between the $Q = 1/2$ subharmonic response and this large-scale mode makes it stable.

This symmetry consideration can be described for a simpler system exhibiting subharmonic instability, for instance a pendulum parametrically driven at twice its natural frequency: if the forcing is strong enough, the pendulum becomes unstable and can oscillate at half the driving frequency. This subharmonic response is symmetric about the zero-angle unstable solution. However, if the pendulum is parametrically driven at its natural frequency, it can oscillate at the driving frequency but then makes a non-zero angle on temporal average: the harmonic response is generically coupled to the temporal harmonic zero, which corresponds to a constant non-zero angle.

Dynamos generated by cellular flows have been found either harmonic or subharmonic at twice the wavelength of the flow. It has been shown by Matthews (1999) that the most unstable magnetic mode generated by a simple convective flow with two-dimensional rolls in a rotating fluid layer is harmonic and involves a large-scale field, whereas the Couette–Taylor dynamo grows at twice the period of the Taylor cells as observed by Laure, Chossat & Daviaud (2001). Dynamo action by Roberts flows, i.e. flows depending periodically on two Cartesian coordinates and independent of the third one, has been studied by Tilgner & Busse (1995) and Plunian & Radler (2002). Harmonic magnetic fields are the most unstable in large enough systems and involve a large-scale component.

Note that when Q is very small, we expect to recover the results obtained for $Q = 0$, which we called the harmonic response. How small does Q have to be for the solution to resemble the harmonic solution? When $Q \neq 0$, the longest Fourier component of the eigenmode has wavenumber Q. For localized shear at $z = 0$, this Fourier component is damped vertically on a skin depth $(RmQ)^{-1/2}$. Provided this skin depth is very large, the Fourier mode Q has a vertical structure similar to an x-independent mode. This requires $Q \ll 1/Rm$. Because the critical magnetic Reynolds number is larger than $\sim 10^3$ for localized shear at $z = 0$, Q must be very small to recover the harmonic response, at most $Q \simeq 10^{-3}$. We checked that for values of Q much smaller than $1/Rm$, the critical magnetic Reynolds number is close to the value computed for the harmonic response. However, once Q became of the order of $1/Rm$ or larger, we could not find any unstable modes.

Such low but non-zero values of Q are not relevant to experimental studies. An experimental device typically has $\sim$10 ferromagnetic blades, so we focused on $Q > 1/10$ when discussing the subharmonic response. The VKS experiment has cylindrical geometry, and if a comparison is to be made, the x-direction of these computations would correspond to the azimuthal direction of cylindrical coordinates. With eight ferromagnetic blades, the lowest allowed values for Q are $Q = 0$, for the axisymmetric component, followed by $Q = 1/8$. $Q = 0$ corresponds to the harmonic response described in the present study.

7.2. *Bypassing anti-dynamo theorems*

The dynamo flows of the present study are of striking simplicity. Without magnetic permeability modulation, an anti-dynamo theorem discards planar flows (i.e. velocity fields with one vanishing Cartesian component) as candidates to produce a dynamo (Zel'dovich 1957). The cylindrical equivalent is the Cowling theorem (Cowling 1933): there is no purely axisymmetric dynamo magnetic field. A broader version of this theorem is proven in Ivers & James (1984): even if the fluid is compressible, and the magnetic field time-dependent, and if electrical conductivity and magnetic permeability are space-dependent but axisymmetric, there cannot be an axisymmetric dynamo magnetic field. Taking the limit of an infinite radius of curvature, the extension to the planar situation seems rather straightforward: if the velocity field, electrical conductivity, magnetic permeability and magnetic field are independent of the same Cartesian coordinate, the magnetic field cannot be sustained by dynamo action.

We bypass the first anti-dynamo theorem by imposing a spatial modulation of magnetic permeability, and the second one by assuming that the magnetic field depends on the three spatial coordinates.

Appendix A. Numerical method

The numerical method uses spectral decomposition in the x-direction and finite differences in z. Let us decompose the fields into Fourier series in x:

$$H_x = \sum_{n=-\infty}^{n=+\infty} u_n(z)\mathrm{e}^{\mathrm{i}nx} \quad \text{and} \quad H_z = \sum_{n=-\infty}^{n=+\infty} v_n(z)\mathrm{e}^{\mathrm{i}nx}. \tag{A 1}$$

The projection of (2.4) and (2.5) onto each of the Fourier modes leads to a system of linear ordinary differential equations in z which couple the functions $(u_n)_{n\in\mathscr{Z}}$ and $(v_n)_{n\in\mathscr{Z}}$. The boundary conditions at $z = -D$ and $z = 0$ have been computed and couple these functions as well. The procedure consists of truncating the differential system to $n \in \{-N, \ldots, N\}$ and solving the obtained system with finite differences in z. Each function u_n is decomposed onto P uniformly spaced grid points: $u_n^{(p)} = u_n(-D + pdz)$, with $dz = D/P$ and $p \in \{1, \ldots, P\}$. The v_n functions are decomposed onto $P + 1$ uniformly spaced grid points: $v_n^{(p)} = v_n(-D + (p-1)dz)$, $p \in \{1, \ldots, P+1\}$. The linear operators of the two equations (2.4) and (2.5) (such as multiplication by $\mu_r(x)$ or its derivatives, derivation with respect to x or z, etc.) can be written as matrices of size $((2N+1)(2P+1))^2$ acting on the vector $\boldsymbol{V} = (u_{-N}^{(1)}, \ldots, u_N^{(1)}, u_{-N}^{(2)}, \ldots, u_N^{(2)}, \ldots, u_{-N}^{(P)}, \ldots, u_N^{(P)}, v_{-N}^{(1)}, \ldots, v_N^{(1)}, \ldots, v_{-N}^{(P+1)}, \ldots, v_N^{(P+1)})$, which has $(2N+1)(2P+1)$ coefficients. The boundary coefficients of the matrices representing z-derivatives are obtained using the boundary conditions. The linear system of equations to be solved now reads

$$sMV = \boldsymbol{R}(s)V, \tag{A 2}$$

where matrix $\boldsymbol{R}$ depends upon s. One can then use a test value s_0 to get the eigenvalue s_1, solution to the problem $s_1 MV = \boldsymbol{R}(s_0)V$. This value s_1 is re-injected into matrix $\boldsymbol{R}$ before repeating this step. This process converges in a few iterations to a value of s solving (A 2). When N and P are large enough, the value of s is converged and independent of the resolution.

Appendix B. Boundary conditions at $z = 0$ in the weak modulation limit

After replacing μ_r at the denominator by m_0, the x-averaged boundary condition (2.11) gives

$$\begin{aligned} & a\left[-\epsilon(k^2+m_0 s)\sinh\left(\sqrt{k^2+1+m_0 s}D\right)\right. \\ & \left. -\ m_0\epsilon\sqrt{k^2+s}\sqrt{k^2+1+m_0 s}\cosh\left(\sqrt{k^2+1+m_0 s}D\right)\right] \\ & +d\left[m_0\epsilon\sqrt{k^2+s}\cosh\left(\sqrt{k^2+1+m_0 s}D\right)\right] \\ & +\tilde{H}_z\left[2\sqrt{k^2+m_0 s}\sinh\left(\sqrt{k^2+m_0 s}D\right)\right. \\ & \left. +\ 2m_0\sqrt{k^2+s}\cosh\left(\sqrt{k^2+m_0 s}D\right)\right]=0. \end{aligned} \tag{B 1}$$

The same boundary condition written for harmonic $+1$ (that is $\mathrm{e}^{\mathrm{i}x}$) leads to

$$\begin{aligned} & \tilde{H}_x\left[\epsilon(k^2+1+m_0 s)\sinh\left(\sqrt{k^2+m_0 s}D\right)\right. \\ & \left. +\ m_0\epsilon\sqrt{k^2+1+\mathrm{i}Rm+s}\sqrt{k^2+m_0 s}\cosh\left(\sqrt{k^2+m_0 s}D\right)\right] \\ & +a\left[-\sqrt{k^2+1+\mathrm{i}Rm+s}\frac{m_0\epsilon^2}{2\mathrm{i}}\sqrt{k^2+1+m_0 s}\cosh\left(\sqrt{k^2+1+m_0 s}D\right)\right] \\ & +c\left[\sqrt{k^2+1+m_0 s}\sinh\left(\sqrt{k^2+1+m_0 s}D\right)\right. \\ & \left. +\ m_0\sqrt{k^2+1+\mathrm{i}Rm+s}\cosh\left(\sqrt{k^2+1+m_0 s}D\right)\right] \\ & +d\left[-\mathrm{i}\sqrt{k^2+1+m_0 s}\sinh\left(\sqrt{k^2+1+m_0 s}D\right)\right. \\ & \left. -\ \mathrm{i}m_0\sqrt{k^2+1+\mathrm{i}Rm+s}\cosh\left(\sqrt{k^2+1+m_0 s}D\right)\right] \\ & +\tilde{H}_z\left[-\mathrm{i}m_0\epsilon\sqrt{k^2+1+\mathrm{i}Rm+s}\cosh\left(\sqrt{k^2+m_0 s}D\right)\right]=0. \end{aligned} \tag{B 2}$$

The equation for harmonic -1 is the same but with i replaced by $-\mathrm{i}$, and leaving s unchanged (although s is pure imaginary at onset). The x-average of boundary condition (2.10) yields

$$\begin{aligned} & \tilde{H}_x 2\sqrt{k^2+m_0 s}\left[-\sinh\left(\sqrt{k^2+m_0 s}D\right)-\cosh\left(\sqrt{k^2+m_0 s}D\right)\right] \\ & +a\left[-m_0 Rm\epsilon\sqrt{k^2+1+m_0 s}\cosh\left(\sqrt{k^2+1+m_0 s}D\right)\right] \\ & +dm_0 Rm\epsilon\cosh\left(\sqrt{k^2+1+m_0 s}D\right) \\ & +\tilde{H}_z 2m_0 Rm\cosh\left(\sqrt{k^2+m_0 s}D\right)=0. \end{aligned} \tag{B 3}$$

Harmonic $+1$ of boundary condition (2.10) gives:

$$\begin{aligned}
&\tilde{H}_x \left[\mathrm{i}\epsilon(1+m_0 s)\sqrt{k^2+1+\mathrm{i}Rm+s}\sinh\left(\sqrt{k^2+m_0 s}D\right)\right.\\
&\left.+(\mathrm{i}(1+s)-Rm)m_0\epsilon\sqrt{k^2+m_0 s}\cosh\left(\sqrt{k^2+m_0 s}D\right)\right]\\
&+a\left[\left(1-\mathrm{i}\frac{Rm-\mathrm{i}}{2}m_0\epsilon^2\right)\sqrt{k^2+1+m_0 s}\cosh\left(\sqrt{k^2+1+m_0 s}D\right)\right.\\
&\left.+\sqrt{k^2+1+iRm+s}\sinh\left(\sqrt{k^2+1+m_0 s}D\right)\right]\\
&+b\left[-\mathrm{i}\sqrt{k^2+1+m_0 s}\cosh\left(\sqrt{k^2+1+m_0 s}D\right)\right.\\
&\left.-\ \mathrm{i}\sqrt{k^2+1+\mathrm{i}Rm+s}\sinh\left(\sqrt{k^2+1+m_0 s}D\right)\right]\\
&+c\left[(\mathrm{i}(m_0-1)-m_0 Rm)\cosh\left(\sqrt{k^2+1+m_0 s}D\right)\right]\\
&+d\left[((m_0-1)+\mathrm{i}m_0 Rm)\cosh\left(\sqrt{k^2+1+m_0 s}D\right)\right]\\
&+\tilde{H}_z\left[-\mathrm{i}m_0\epsilon(\mathrm{i}-Rm)\cosh\left(\sqrt{k^2+m_0 s}D\right)\right]=0, \qquad \text{(B 4)}
\end{aligned}$$

and the equation for harmonic -1 is the same but with i replaced by $-\mathrm{i}$, and leaving s unchanged.

REFERENCES

BUSSE, F. H. & WICHT, J. 1992 A simple dynamo caused by conductivity variations. *Geophys. Astrophys. Fluid Dyn.* **64**, 135–144.

COWLING, T. G. 1933 The magnetic field of sunspots. *Mon. Not. R. Astron. Soc.* **94**, 39–48.

GALLET, B., PÉTRÉLIS, F. & FAUVE, S. 2012 Dynamo action due to spatially dependent magnetic permeability. *Europhys. Lett.* **97**, 69001.

GIESECKE, A., STEFANI, F. & GERBETH, G. 2010 Role of soft-iron impellers on the mode selection in the von Kármán sodium dynamo experiment. *Phys. Rev. Lett.* **104**, 044503.

GILBERT, A. D. 1988 Fast dynamo action in the Ponomarenko dynamo. *Geophys. Astrophys. Fluid Dyn.* **44**, 241–258.

GISSINGER, C. 2009 A numerical model of the VKS experiment. *Europhys. Lett.* **87**, 39002.

GUCKENHEIMER, J. & HOLMES, P. 1986 *Nonlinear Oscillations, Dynamical Systems and Bifurcations of Vector Fields*. Springer.

IVERS, D. J. & JAMES, R. W. 1984 Axisymmetric antidynamo theorems in compressible non-uniform conducting fluids. *Phil. Trans R. Soc. Lond.* A **312**, 179–218.

KNOBLOCH, E. & SILBER, M. 1990 Travelling wave convection in a rotating layer. *Geophys. Astrophys. Fluid Dyn.* **51**, 195–209.

LARMOR, J. 1919 How could a rotating body such as the sun become a magnet?. In *Rep. 87th Meeting Brit. Assoc. Adv. Sci., Bornemouth, Sept. 9–13*, pp. 159–160. John Murray.

LAURE, P., CHOSSAT, P. & DAVIAUD, F. 2001 Generation of magnetic field in the Couette–Taylor system. In *Dynamo and Dynamics, a Mathematical Challenge* (ed. P. Chossat, D. Ambruster & I. Oprea). pp. 17–24. Kluwer.

LORTZ, D. 1968 Impossibility of dynamos with certain symmetries. *Phys. Fluids* **11**, 913–915.

MATTHEWS, P. C. 1999 Dynamo action in simple convective flows. *Proc. R. Soc. Lond.* A **455**, 1829–1840.

MONCHAUX, R., BERHANU, M., AUMAÎTRE, S., CHIFFAUDEL, A., DAVIAUD, F., DUBRULLE, B., RAVELET, F., FAUVE, S., MORDANT, N., PÉTRÉLIS, F., BOURGOIN, M., ODIER, P., PINTON, J.-F., PLIHON, N. & VOLK, R. 2009 The von Kármán sodium experiment: turbulent dynamical dynamos. *Phys. Fluids* **21**, 035108.

PÉTRÉLIS, F., MORDANT, N. & FAUVE, S. 2007 On the magnetic fields generated by experimental dynamos. *Geophys. Astrophys. Fluid Dyn.* **101**, 289–323.

PLUNIAN, F. & RADLER, K. H. 2002 Subharmonic dynamo action in the Roberts flow. *Geophys. Astrophys. Fluid Dyn.* **96**, 115–133.

SIEMENS, C. W. 1867 On the conversion of dynamical into electrical force without the aid of permanent magnetism. *Proc. R. Soc. Lond.* **15**, 367–369.

STEFANI, F., XU, M., GERBETH, G., RAVELET, F., CHIFFAUDEL, A., DAVIAUD, F. & LÉORAT, J. 2006 Ambivalent effects of added lid layers on steady kinematic dynamos in cylindrical geometry: application to the VKS experiment. *Eur. J. Mech.* B/Fluids **25**, 894–908.

TILGNER, A. & BUSSE, F. H. 1995 Subharmonic dynamo action of fluid motions with two-dimensional periodicity. *Proc. R. Soc. Lond,* A **448**, 237–244.

WICHT, J. & BUSSE, F. H. 1994 Dynamo action induced by lateral variation of conductivity. In *Solar and Planetary Dynamos* (ed. M. R. E. Proctor, P. C. Matthews & A. M. Rucklidge), pp. 329–338. Cambridge University Press.

ZEL'DOVICH, YA. B. 1957 The magnetic field in the two-dimensional motion of a conducting turbulent fluid. *Sov. Phys. JETP* **4**, 460–462.